SciEn
Journal of Engineering Advancements Vol. 04(04) 2023, pp 116-123 https://doi.org/10.38032/jea.2023.04.002

Optimal Tuning of a LQR Controlled Active Quarter Car System Using Global Best Inertia Weight Modified Particle Swarm Optimization Algorithm

Oghenenyoreme Emakpo Agbroko, Erastus Olarewaju Ogunti

Department of Electrical and Electronics Engineering, Federal University of Technology, Akure, Ondo State, Nigeria

Received: April 10, 2023, Revised: October 28, 2023, Accepted: October 28, 2023, Available Online: November 22, 2023

ABSTRACT

A key factor in the design of a car is the comfort and safety of its passengers. The quarter-car suspension system is a feature of the car that ensures load-carrying capacity as well as comfort and safety. It comprises links, springs, and shock absorbers (dampers). Due to its significance, several research has been conducted, to increase its road handling and holding capability while trying to keep its cost moderate. To enhance customer comfort and load carrying, the road holding capacity of an active quarter car suspension was improved/controlled in this study, using the Global Best Inertia Weight Modified Particle Swarm Optimization Algorithm. The observation of the closed loop and open loop systems after designing and simulating on MATLAB reveals a significant improvement in the closed loop system's road holding ability compared to the open loop, in that, when the system was subjected to pothole, the deflection of sprung mass reached steady state in 37.37 seconds as opposed to 7000 seconds for the open loop.

Keywords: Quarter Car, Linear Quadratic Regulator (LQR), Road profile, Global Best Inertia Weight Modified Particle Swarm Optimization (GBbest-IWM-PSO) Algorithm

1 Introduction

A mechanism that physically separates a vehicle's body from its wheels is known as a quarter car system or automobile suspension system. By eliminating body vibration, roll, and heave of the body through an appropriate road contact for the tires [1], it significantly contributes to the safety and comfort of the vehicle's occupants by operating as a low pass fitter (LPF). Basically, it consists of (a) an elastic component, usually a coil spring, that transmits a force proportional to and in the opposite direction of the elongation of the suspension and supports the entire static load. (b) a damping component (typically a hydraulic shock absorber), which delivers a dissipative force opposite to the elongation speed and proportional to it; this component [2], [3] delivers a negligible force at steady-state but is essential to the dynamic behavior of the suspension; and (c) a set of mechanical components that connect the suspended (sprung) body to the un-sprung (tires and wheels) mass [4].

Linear quadratic regulator (LQR) is an optimal control technique that uses a state space representation model as its foundation. It is designed by utilizing linear optimization methods. LQR controllers are designed for multi-variable and dynamic systems that are both linear and sometimes non-linear [5]. It has applications in a variety of fields, including aerospace systems [6], high-performance motion control applications for direct current (DC) motors [7], unmanned aerodynamic vehicles (UAV) [8], control of radar antenna systems [2], and autopilots for racing yachts [9]. The state weighting matrix Q and the control weighting matrix 'R' are two factors that determine its performance. Tuning LQR to attain optimality, is laborious and time-consuming when using traditional control methods [6]. Hence, to find the best values for Q and R, researchers have used a variety of evolutionary optimization techniques, including the Bees Algorithm (BA), Genetic Algorithm (GA), and Particle Swarm Optimization (PSO) Algorithm, among others, to identify the best weighting matrices for LQR controllers [10], [5], and [11]. PSO has surpassed other computational techniques like GA and BA [12]-[14]. This is primarily because it is easy to implement, converges quickly, is robust to control parameters, and is computationally efficient [15]. However, it has the drawback of having its particles imprisoned in a local minimum as opposed to a global minimum, making the local minimum to be the outcome. As a result, the Global Best Inertia Weight Modified PSO (Gbest-IWM-PSO) algorithm, among other variants of PSO, was implemented [16].

Gbest-IWM-PSO was utilized in this study to optimize the tuning of an LQR-controlled quarter-car system. The resultant system was then exposed to various road conditions to examine its road-holding performance for providing comfort for its occupants and the safety of cargo.

2 Concept and Review of Related Works

To ensure the safety of goods/loads within the car and the comfort of the human occupants, a quarter-car suspension system functions as an LPF. When a disturbance of any kind occurs, the goal is to maximize the LPF characteristics of the suspension system using an LQR and then optimize the LQR performance using Gbest-IWM-PSO. This ensures that the system recovers its stability as quickly as possible. Quarter car suspension systems are of three types: active, semi-active, and passive. The spring, damper (shock absorber), and linkages [17]-[20] make up the passive suspension. By selecting an appropriate spring stiffness and damping coefficient—a measure of the shock absorber characteristics—a suitable system response can be achieved [21]. Passive systems feature set specifications that need to be selected to provide a balance between load-carrying capacity, road handling, and ride comfort. A "soft" suspension is used to maintain contact between the vehicle body and the tires to

*Corresponding Author Email Address: everestagbroko@gmail.com

produce ride comfort. Road disturbances are readily absorbed by the "soft" suspension. Because of this, "soft" suspensions are used in most luxury vehicles to give a smooth ride. The road handling of a vehicle is its second performance attribute. This describes a vehicle's capacity to keep its tires in contact with the ground during turns and other dynamic maneuvers. This is possible with "stiff" suspension like those seen in sports vehicles. Finding the ideal compromise between the two vehicle performance characteristics that will best serve the intended customer, is the task of a passive suspension system designer [1]. See Fig. 1. As demonstrated in Fig. 2, active suspension is an intelligent system that incorporates sensors, actuators, microcontrollers, and other components, as opposed to passive systems. As a result, it can adjust its stiffness and damping coefficient to suit the state of the road. Additionally, it has the capacity to add or take away energy from the system. Its drawbacks include the necessity for a significant amount of external energy to create the required control force [22], high cost, complex design, and propensity for oscillation (instability).

With just a fraction of the power usage of active suspension systems, semi-active suspension systems can give the same versatility, adaptability, and improved performance while maintaining the reliability of their passive counterparts. The damping or spring coefficients of a semi-active suspension can typically be adjusted in real-time as depicted in Fig. 3. The semi-active control devices do not lose stability, unlike active suspension systems, because they cannot input mechanical energy into the control system. These devices include hydro-pneumatic, hydro-elastic, and hydra gas suspensions as well as air springs, switchable shock absorbers, dampers with controllable fluids (such as electrorheological and magnetorheological fluids), various self-leveling solutions, and dampers with controllable fluids [22].

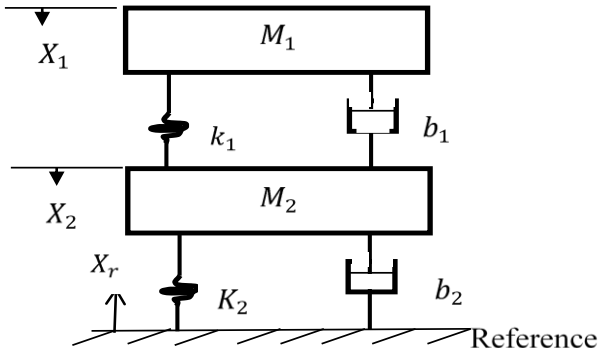

Fig. 1 Passive Suspension System

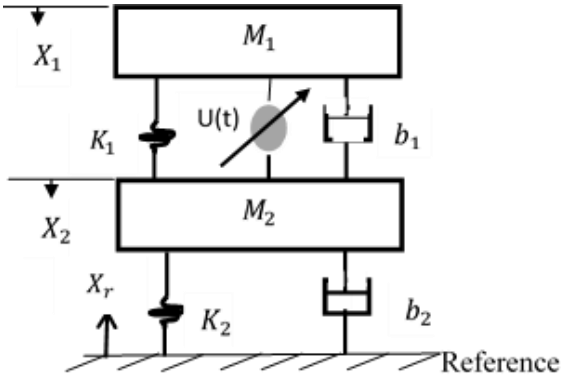

Fig. 2 Active Suspension System

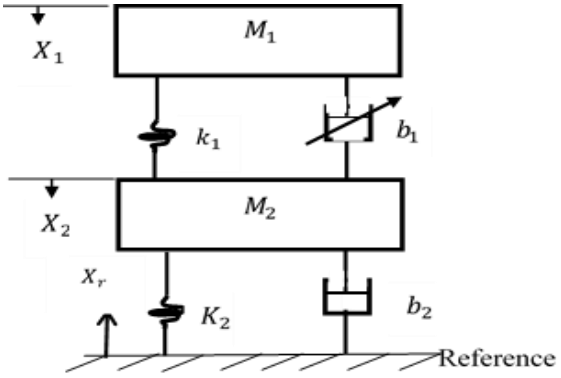

Fig. 3 Semi-Active Suspension System

Numerous control strategies have been used to enhance the damping and spring coefficient of both active and semi-active systems. These include the optimization of sliding mode control of Quarter vehicle using fuzzy logic [23], utilization of a fuzzy controller that is tuned by PSO to optimize an active suspension model [20], using fuzzy PID and LQR to optimize a Quarter car system [18], and Adaptive Fuzzy Logic control for a semi-active suspension model [24].

Eberhart and Kennedy's 1995 study yielded Particle Swarm Optimization [25]. Craig Reynolds first came up with the concept in 1987 and proposed three flocking rules to perform the mimicked bird behavior [26]. PSO computation consists of five fundamental stages. They are (i) problem definition (ii) parameter setup (iii) position and velocity initialization (iv) PSO main loop and (v) results presentation. There are four steps in PSO main loop: (a) Function evaluation (b) Personal best and global best computation (c) updating position and velocity, and (d) storing the best values (Fig. 4).

The equation for updating the velocity of Gbest-IWM-PSO, as proposed by Arumugan and Rao [16] is,

$$V_i^{t+1} = \left(1.1 - \frac{Gbest}{Pbest}\right) \times V_i^t + C_1 \times rand_1 \times (Pbest - V_i^t) + C_2 \times rand_2 \times (Gbest - V_i^t) \quad (1)$$

And Eq. (2) is for updating particle position [25],

$$X_i^{t+1} = X_i^t + V_i^{t+1} \quad (2)$$

Where V_i^{t+1} is the present particle velocity, X_i^{t+1} is the present particle position, Gbest is the global best position, Pbest is the personal best position, V_i^t is the previous particle velocity, X_i^t is the previous particle position, C_1 and C_2 are the personal and social acceleration coefficients, $rand_1$ and $rand_2$ are random variables between one and four.

3 Research Method

With respect to the block diagram of an active Quarter car system in Fig. 2 and applying Newton's law of motion which is,

$$F = ma \quad (3)$$

where F is force (Newton), m is mass (g) and a is acceleration (m/s^2).

$$U(t) = M_1\ddot{X}_1 + b_1(\dot{X}_1 - \dot{X}_2) + k_1(X_1 - X_2) \quad (4)$$

$$-U(t) = M_2\ddot{X}_2 + b_2(\dot{X}_2 - \dot{X}_r) + b_1(\dot{X}_2 - \dot{X}_1) + k_2(X_2 - X_r) + k_1(X_2 - X_1) \quad (5)$$

where M_1 is the sprung mass, which is a quarter of the mass of the vehicle. The mass of tire and wheel is M_2, also referred to as the un-sprung mass. k_1 and k_2 are the spring coefficient of the sprung and un-sprung mass respectively while b_1 and b_2 represent the damping coefficient of the sprung and un-sprung mass. From Eqs. (4), (5), $\dot{X}_1$ - $\dot{X}_2$ represent the deflection of the sprung mass, $\dot{X}_1$is the speed of the car body, $\ddot{X}_1$ represents the acceleration of the car body, $X_2 - X_r$ is the deflection of the tire, $\dot{X}_2$ is the tire velocity and U(t) is the actuating signal. Values of quarter car parameters are shown in Table 1.

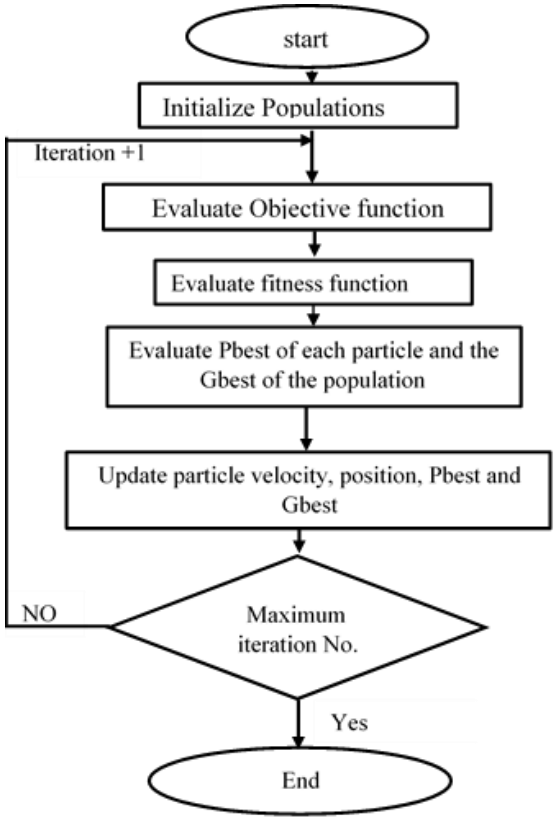

Fig. 4 Flow Chart of Basic PSO Algorithm (Adapted from [6])

Table 1 Quarter Car suspension parameters (Source: [18])

Symbol	Parameter	Value/unit
M_1	A quarter of Bus body Mass	300kg
M_2	Un-sprung Mass (Tire and Wheel)	59kg
k_1	Spring coefficient of the suspension system	17,000 N/m
k_2	Spring coefficient of wheel and tire	180,000 N/m
b_1	The damping coefficient of the suspension system	500 N.s/m
b_2	Damping coefficient of tire and wheel	1050 N.s./m

Consider an LTI (Linear Time Invariant) system whose block diagram is shown in Fig. 5,

$$\dot{x} = Ax + Bu \tag{6}$$

$$y = Cx + Du \tag{7}$$

Where A is the nxn state matrix, B is the nxr input matrix, C is the mxn output matrix, D is mxr direct transmission matrix, x is the nx1 state vector, $\dot{x}$ is the nx1 derivative of the state vector, y is the mx1 output vector and u is the rx1 input vector.

An objective of this research is to determine an OPTIMAL value of K that will minimize the cost function (J) of an LQR controller.

$$J = \frac{1}{2}\int_{t_0}^{t_f} (x^T Qx + u^T Ru)dt \tag{8}$$

Where t_f is the final time, $t_0$is the initial time, Q is the State weighting matrix which is a positive semi-definite nxn matrix and R is the control weighting matrix which is a positive definite matrix.

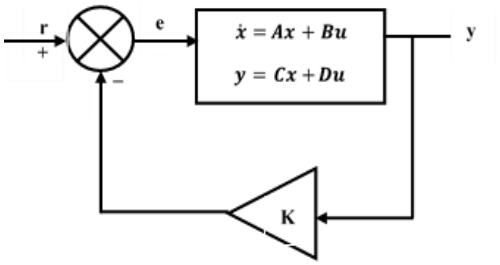

Fig. 5 Block diagram of an LTI system

At optimal state,

$$u^* = -Kx \tag{9}$$

and

$$K = R^{-1}B^T P \tag{10}$$

where u^* is the system input that minimizes the objective function, K is the optimal control feedback matrix and P is the solution of the Algebraic Riccati Equation (ARE) shown in Eq. (11).

$$PA + A^T P + Q - PBR^{-1}B^T P = 0 \tag{11}$$

The performance index that was used as the objective function of Gbest-IWM-PSO to achieve the minimization of the cost function (J) was Integral Time Square Error (ITSE) i.e.

$$ITSE = \int t(e^2)dt \tag{12}$$

where e is the error signal (Fig. 5) which is,

$$e = r - ky \tag{13}$$

where r is the reference input and y is the system output.

Fig. 6 shows a block diagram of a full-state feedback controller with variable Gain (K). Gbest-IWM-PSO was used to vary the value of K for each iteration (ie for each iteration, the Global best particle position is equal to K). After the final iteration, the overall Global best particle position which is the position that best optimizes the objective function, was equated to K. Finally, with the aid of Eqs. (10), (11), the values of Q and R were determined.

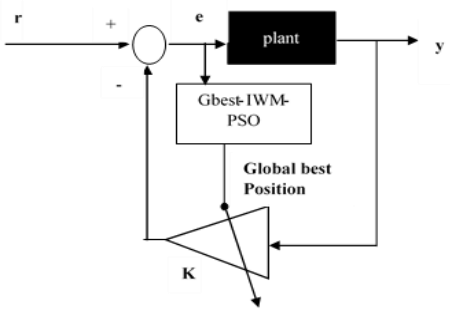

Fig. 6 Full State Feedback Controller

The Quarter car model was designed on MATLAB Simulink while the Gbest-IWM-PSO was computed using MATLAB EDITOR. With the aid of the "TO WORKSPACE" block, MATLAB "sim" command, and "logsout" command, the Simulink model and EDITOR were made to interact. Twenty runs with fifty iterations per run were used to simulate the system on the MATLAB 2020b version. Table 2 shows the Gbest-IWM-PSO parameters used for the simulation.

Table 2 Gbest-IWM-PSO parameters

s/n	Item	Value	Unit
1	C_1	2	constant
2	C_2	2	constant
3	n	4	number
4	vsize	[1 n]	1xn matrix
5	pop	20	number

In Table 2 n is the number of decision variables, vsize is the matrix size of the decision variable, pop is the particle population, the lower bound (LB) of the search space is [-1000 -1000 -1000 -1000], while the upper bound is [100000 100000 100 100].

ROAD PROFILE: Three road conditions were used as a test signal for this research and they are Pot Hole Signal. This is represented with a step signal, with its step time set at 50 seconds. It will be better understood by assuming an automobile tire coming out of a pot hole Fig. 7.

Speed Breaker-The design layout as shown in Fig. 8, is a combination of the sine wave, step signal, and a product block to form a bump input as depicted in Fig. 9 [18].

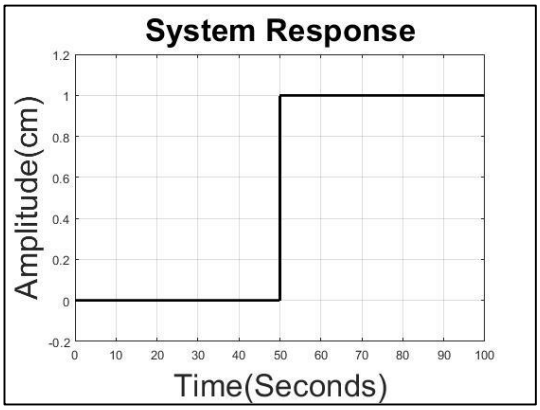

Fig. 7 Pot Hole

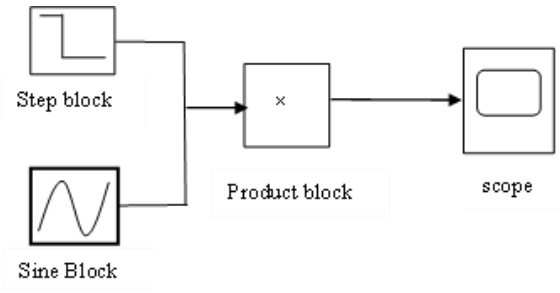

Fig. 8 Block diagram of speed breaker design

Rough Road- A sine wave signal was used to represent rough road (uneven pavement) Fig. 10. For the rough road, there was disturbance throughout the simulation time, unlike the other two road conditions where the disturbance to the system occurred at an instant of time within the simulation period.

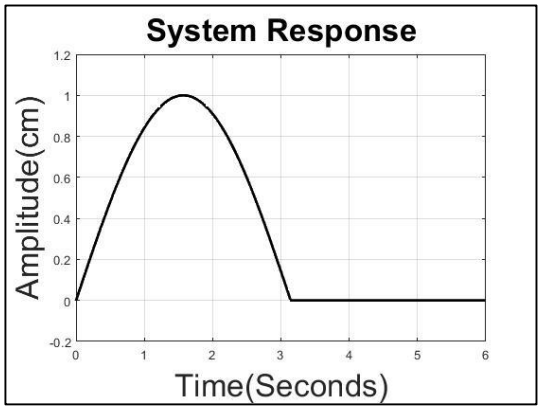

Fig. 9 Speed Breaker

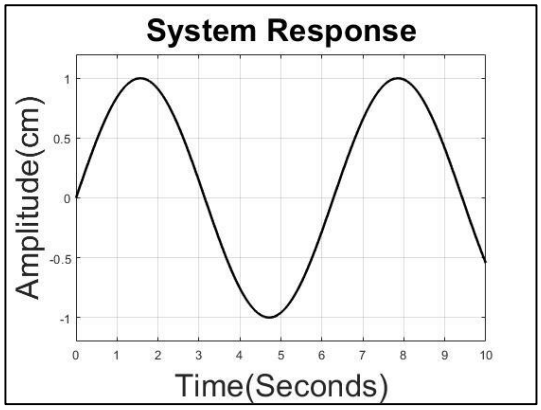

Fig. 10 Rough Road

4 Results and Discussion

Results from the simulation include:

G_{best} is [66361 43157 -477 -195],

R is $\frac{1}{122.1343} \times 10^{-6}$, Q is $\begin{bmatrix} 1 & 0 & 0 & 0 \\ 0 & 22 & 0 & 0 \\ 0 & 0 & 1 & 0 \\ 0 & 0 & 0 & 7 \end{bmatrix}$,

P is $\begin{bmatrix} 14.2359 & 9.0649 & -39.1704 & 0.241 \\ 9.0649 & 170.4281 & -3.8804 & -8.5679 \\ -39.1704 & -3.8804 & 447.5057 & 0.0808 \\ 0.241 & -8.5679 & 0.0808 & 133.863 \end{bmatrix}$

With respect to Abdussalam [18]:

R was 0.0001, K was [0.0295 0.3072 -2.5105 -0.2029] × 10^4 and

Q was $\begin{bmatrix} 1000 & 0 & 0 & 0 \\ 0 & 1000 & 0 & 0 \\ 0 & 0 & 1000 & 0 \\ 0 & 0 & 0 & 1000 \end{bmatrix}$,

Furthermore, Abdussalam [18], made a graphical comparison between the speed breaker responses of a fuzzy PID-controlled system, an LQR controlled system, and a system without control (No numerical was analysis given). Careful observation of the graphs reveals that his LQR controlled system contains more oscillation during the transient period, with very much higher peak and trough overshoot. It however had a smaller settling time, peak time, and trough time when compared to the Gbest-IWM-PSO tuned LQR controlled Quarter car system in this research work.

DofSM is the deflection of sprung mass, VofSM is the velocity of sprung mass, DofUM is the deflection of un-sprung mass and VofUM is the velocity of un-sprung mass Table 3-Table 8. With regards to the open loop response to pothole and

considering the deflection of sprung mass, the system attained a maximum peak value of 1.28113×10^{-4}cm at a time of 13.714 secs, a maximum trough of 1.24436×10^{-6}cm at a time of 27.633secs, with a settling time of 7000secs, rise time of 6.835 secs and a steady state value of 6.428×10^{-4}cm. As regards the velocity of sprung mass, the maximum peak to trough was 1.45569×10^{-5} cm/s to -1.44231×10^{-5}cm/s, at a time of 6.736 and 20.636 secs respectively. Steady state value of 0 with settling time of 6666.67secs. For the deflection of un-sprung mass, the maximum peak was 1.09772×10^{-5}cm at a time of 14.785secs, a maximum trough of 8.67906×10^{-8}cm at a time of 28.225secs, a rise time of 6.553secs, and a steady state value of 5.257×10^{-6}cm. Whereas, for the velocity of un-sprung mass, the maximum peak was 1.11×10^{-6}cm/s at a time of 7.977secs, the maximum trough was -1.368×10^{-6}cm/s at a time of 21.368secs, settling time of 4509.3seconds with a steady state value of 0. Fig. 11 and Table 3.

As regards the open loop response to the speed breaker, considering the deflection of sprung mass, the maximum peak of the system was 2.8643×10^{-5}cm at a time of 8.07 secs, maximum trough of -2.84808×10^{-5} at a time of 22.28secs, and settling time of 7649.15secs. While for the velocity of sprung mass, the maximum peak to trough value was 6.1656×10^{-6}cm/s to -6.50222×10^{-6}cm/s at a time of 2.897secs and 15.253secs respectively, with a settling time of 7000secs. For the deflection of un-sprung mass, the maximum peak was 2.60477×10^{-6}cm, the maximum trough was -2.55277×10^{-6}cm, the peak time was 7.783secs, trough time of 22.535secs and the settling time of 5000secs. While for the velocity of un-sprung mass, the maximum peak was 7.65148×10^{-7}cm/s, maximum trough of -7.71073×10^{-7}cm/s, peak time of 3.118secs, trough time of 15.295secs and settling time of 4000secs. Table 4 and Fig. 12.

As regards the open loop response of the system to rough road and considering the deflection of sprung mass, the peak time, trough time, and settling time were 5.33secs, 20.26secs, and 5452.23secs respectively.

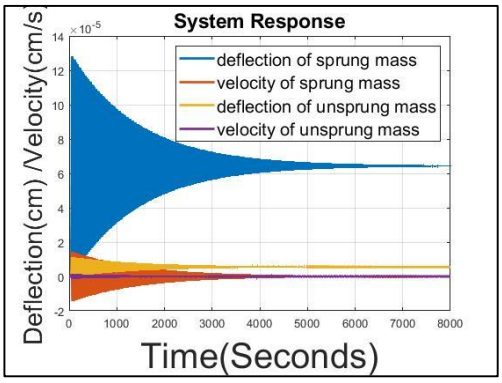

Fig. 11 Open loop pot-hole response

Table 3 Measurements from Open loop pot-hole response

Response	Peak time	Settling time	Rise time	Trough time	Peak	Trough	Steady state value
DofSM	13.714	7000	6.835	27.633	1.2811×10^{-4}	1.2443×10^{-6}	6.428×10^{-4}
VofSM	6.736	6666.67	-	20.636	1.4556×10^{-5}	-1.4423×10^{-5}	0
DofUM	14.785	4110.48	6.553	28.225	1.0977×10^{-5}	8.6790×10^{-8}	5.257×10^{-6}
VofUM	7.977	4509.3	-	21.368	1.11×10^{-6}	-1.368×10^{-6}	0

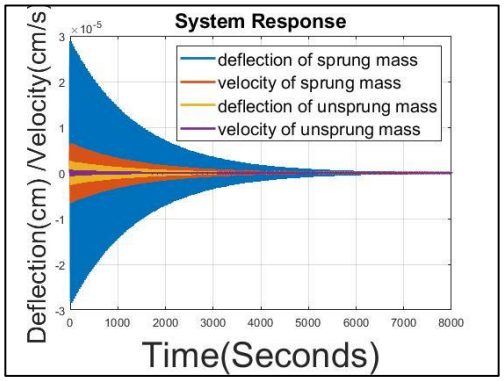

Fig. 12 Open loop speed breaker response

Table 4 Measurements from Open loop speed breaker response

Response	Peak time	Settling time	Trough time	Peak	Trough
DofSM	8.07	7649.15	22.28	2.8643×10^{-5}	-2.84808×10^{-5}
VofSM	2.897	7000	15.253	6.1656×10^{-6}	-6.50222×10^{-6}
DofUM	7.783	5000	22.535	2.60477×10^{-6}	-2.55277×10^{-6}
VofUM	3.118	4000	15.295	7.65148×10^{-7}	-7.71073×10^{-7}

During the transient period, the maximum peak was 1.726×10^{-5}cm while the maximum trough value was 1.85952×10^{-5}cm. The system finally settled with a steady peak to trough value of 3.81717×10^{-6}cm and -3.93×10^{-6}cm. For the velocity of sprung mass, during its transient state, the maximum peak value was 6.115×10^{-6}cm/s at a time 2.8secs, the maximum trough was -6.85539×10^{-6}cm/s at a time of 12.63secs while at steady state, the peak value was 3.64242×10^{-6}cm/s the trough value was -3.644×10^{-6}cm/s and the settling time was 4615secs. With respect to the Deflection of un-sprung mass, the maximum peak was 1.663×10^{-6}cm at a time of 4.68secs, the maximum trough was -1.78517×10^{-6}cm at a time of 20.23secs, attained its steady state with a peak to trough of 4.34159×10^{-7}cm and -4.344×10^{-7}cm respectively, with a settling time of 5037.52secs. For the velocity of un-sprung mass, the maximum peak was 7.618×10^{-7}cm/s, the maximum trough was -7.96102×10^{-7}cm/s, the peak time of 3.33secs, the trough time of 12.25secs, settling time of 4030.65secs with final peak of 4.41081×10^{-7}cm/s and trough value of -4.42×10^{-7}cm/s. Fig. 13 and Table 5.

Concerning the closed loop response to pot-hole, considering the deflection of sprung mass, the system maximum peak was 1.19805cm at a time of 14.15secs, maximum trough value of 0.961823cm at a time of 28.46secs, the rise time of 9.14secs, the system finally settles to a steady state value of 1 at 37.38secs with a steady state error of 0. For the velocity of sprung mass, the maximum peak was 0.14246cm/s, maximum trough value was -0.0279637cm/s, peak time was 5.32secs, trough time was 19.58secs and settling time of 28.14secs. Considering the deflection of un-sprung mass, the maximum peak was 0.105052cm, maximum trough was 0.0820422cm, peak time of 13.76secs, trough time was 28.82secs, rise time of 9.06secs, and settling time of 38.28secs. While for the velocity of un-sprung mass, the maximum peak to trough value was 0.014664cm/sec to -0.00478997cm/s, there was a peak time of 6.09secs, trough time of 17.98secs and settling time of 27.06secs. Fig. 14 and Table 6.

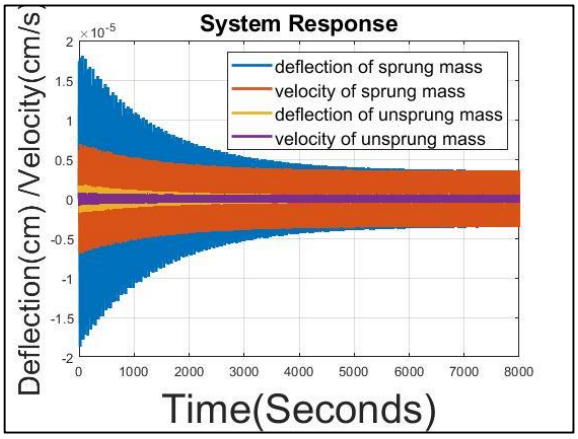

Fig. 13 Open loop rough road response

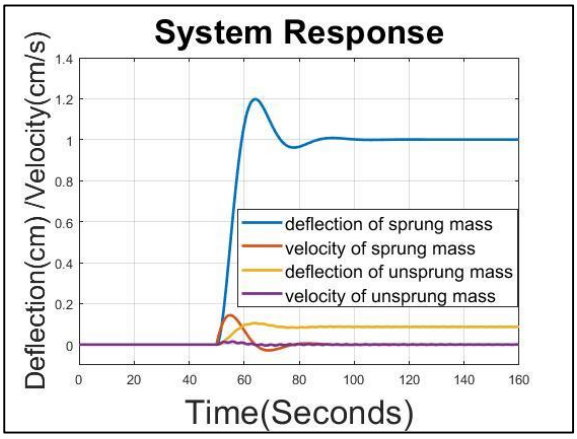

Fig. 14 Closed loop pot-hole response

Table 5 Measurements from Open loop Rough road response

	TRANSIENT STATE				STEADY STATE		
Response	**Peak**	**Trough**	**Peak time**	**Trough time**	**Settling time**	**Peak**	**Trough**
DofSM	1.726×10^{-5}	1.85952×10^{-5}	5.33	20.26	5452.23	3.81717×10^{-6}	-3.93×10^{-6}
VofSM	6.115×10^{-6}	-6.85539×10^{-6}	2.8	12.63	4615	3.64242×10^{-6}	-3.644×10^{-6}
DofUM	1.663×10^{-6}	-1.78517×10^{-6}	4.68	20.23	5037.52	4.34159×10^{-7}	-4.344×10^{-7}
VofUM	7.618×10^{-7}	-7.96102×10^{-7}	3.33	12.25	4030.65	4.41081×10^{-7}	-4.42×10^{-7}

Table 6 Measurements from closed loop pot-hole response

Response	**Peak time**	**Settling time**	**Rise time**	**Trough time**	**Maximum peak**	**Maximum trough**	**Steady state value**
DofSM	14.15	37.38	9.14	28.46	1.19805	0.961823	1
VofSM	5.32	28.14	-	19.58	0.14246	-0.0279637	0
DofUM	13.76	38.28	9.06	28.82	0.105052	0.0820422	0.0861087
VofUM	6.09	27.06	--	17.98	0.014664	-0.00478997	0

With respect to the closed loop response of the system to the speed breaker and considering the deflection of the sprung mass, the maximum peak was 1.47711×10^{-5}cm, the maximum trough was -2.90677×10^{-6}cm, peak time was 6.4secs, trough time was 20.2secs, and a settling time of 48.5secs. As regards the velocity of sprung mass, the maximum trough was-2.10989×10^{-6}cm/s, the maximum peak was 4.51939×10^{-6}cm/s, the peak time was 2.5secs, the trough time was 11.6secs and the settling time was 46.3secs. Considering the deflection of un-sprung mass, the maximum trough was -3.48323×10^{-7} cm, maximum peak 1.38185×10^{-6}cm, peak time of 7.4secs, trough time of 19.7secs, and settling time of 40.9secs. Furthermore, for the velocity of un-sprung mass, the maximum peak was-3.81637×10^{-7}cm/s, the maximum trough was 5.98633×10^{-7}cm/s, the peak time of 3secs, the trough time was 11.6secs and the settling time of 22.6secs. Fig. 15 and Table 7.

Finally, with respect to the closed loop system response to rough road and considering the deflection of sprung mass, the maximum peak was 1.1434×10^{-5}cm, at a time of 4.44secs, maximum trough was -4.92813×10^{-6}cm at a time of 20.12secs. It attained a steady state at 29.56secs with a peak to trough value of 3.4257×10^{-6}cm to -3.44318×10^{-6}cm. For the velocity of sprung mass, maximum peak was 4.5348×10^{-6}cm/s, maximum trough was -4.36965×10^{-6}cm/s, peak time was 2.53secs, trough time was 12.24secs and it reached steady state at 18.78secs, with a peak of 3.37789×10^{-6}cm/s, trough value of -3.38388×10^{-6}cm/s. For the deflection of un-sprung mass, the maximum peak was 1.18334×10^{-6}cm at a time of 4.5secs, the maximum trough was -5.77131×10^{-7}cm at a time of 20.25secs and the system settling time was 29.2secs with a peak value of 4.47008×10^{-7}cm and trough value of -4.40555×10^{-7}cm. Finally, when considering the velocity of un-sprung mass, the maximum peak was 5.96112×10^{-7}cm, and the maximum trough was -5.84252×10^{-7}cm at a time of 2.94 and 12.33secs respectively. It settled at a time of 21.53secs with peak to trough values of 4.96596×10^{-7}cm and -4.81141×10^{-7}cm respectively. Fig. 16 and Table 8.

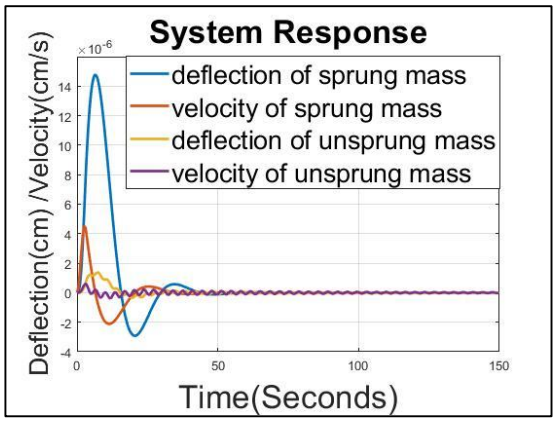

Fig. 15 Closed loop speed breaker response

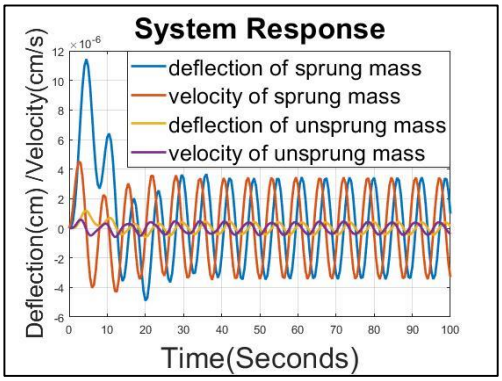

Fig. 16 Closed loop response to rough road

As shown in Fig. 17, the system poles are located at -0.0133 ± j1.8286 and -0.0007 ± j0.2274. Careful observation reveals that the system's dominant poles are the ones located at -0.0007 ± j0.2274. It determines the characteristics of the system; it is located very close to the origin of the s-plane hence resulting in the system oscillating for a long period. Comparing the closed loop pole location (Fig. 18) to that of the open loop shows that the dominant (significant) pole was relocated to -0.1157±j0.2239 whereas there was only a slight effect on the insignificant pole i.e., from -0.0133 ± j1.8286 to -0.014 ± j1.8286. The relocation of the dominant poles far away from the origin of the s-plane resulted in a reduced oscillation time and better system stability and hence better LPF characteristics.

Table 7 Measurements from closed loop response to speed breaker

Response	Peak time	Settling time	Trough time	Peak	Trough
DofSM	6.4	48.5	20.2	1.47711×10^{-5}	-2.90677×10^{-6}
VofSM	2.5	46.3	11.6	4.51939×10^{-6}	-2.10989×10^{-6}
DofUM	7.4	40.9	19.7	1.38185×10^{-6}	-3.48323×10^{-7}
VofUM	3	22.9	11.6	5.98633×10^{-7}	-3.81637×10^{-7}

Table 8 Measurements from closed loop Rough road response

	Transient State				Steady state		
Response	Maximum peak	Maximum trough	Peak time	Trough time	Settling time	Peak	Trough
DofSM	1.1434×10^{-5}	-4.92813×10^{-6}	4.44	20.12	29.56	3.4257×10^{-6}	-3.44318×10^{-6}
VofSM	4.5348×10^{-6}	-4.36965×10^{-6}	2.53	12.24	18.78	3.37789×10^{-6}	-3.38388×10^{-6}
DofUM	1.18334×10^{-6}	-5.77131×10^{-7}	4.5	20.25	29.2	4.47008×10^{-7}	-4.40555×10^{-7}
VofUM	5.96112×10^{-7}	-5.84252×10^{-7}	2.94	12.33	21.53	4.96536×10^{-7}	-4.81141×10^{-7}

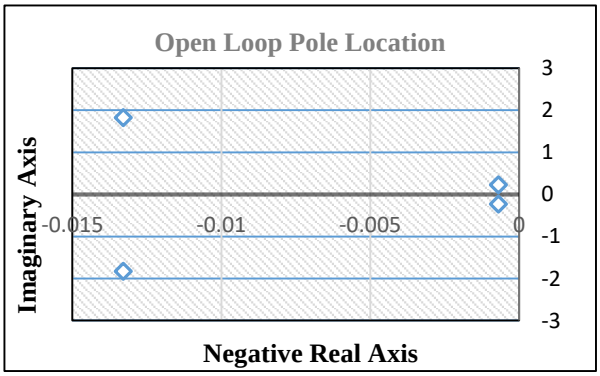

Fig. 17 Open loop pole location

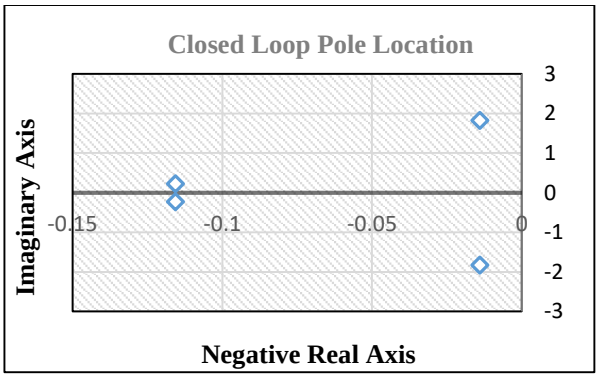

Fig. 18 Closed loop pole location

5 Conclusion

The goal of this research was to maximize the LPF characteristic of an active Quarter car suspension system using Gbest-IWM-PSO optimized LQR. Simulation of the system revealed a relocation of the system dominant (significant) poles from -0.0007 ± j0.2274 to -0.1157 ± j0.2239 resulting in improved transient response of the system, reduced number of oscillations, shorter settling time hence better road holding capacity for passenger comfort and better load carriage. Also noteworthy is the fact that there was a reduction in the amplitude of the maximum peak and trough when considering the system response to speed breaker and rough road. For example, the maximum peak to trough for Deflection of Sprung Mass when considering the speed breaker, for open loop was 0.000028643 to -2.84808×10^{-5} (Fig. 12 and Table 4) while that for closed loop was 1.47711×10^{-5} to -2.90677×10^{-6} (Fig. 15 and Table 7). Furthermore, for the pot hole and considering the deflection of sprung mass, it was observed that the steady state error dropped from 0.9993572cm (i.e. 1- 0.0006428) to 0cm (Table 3 and Table 6).

References

[1] Kashem, S., Nagarajah, R. and Ektesabi, M., 2018. Vehicle suspension systems and electromagnetic dampers. 1st ed. Singapore: Springer Nature, ISBN 9789811054785, pp. 1-175.

[2] Anderson, B. and Moore, J., 1989. Optimal control: linear quadratic methods, Sydney: Prentice-Hall, ISBN 0136386512, pp. 1-374.

[3] Alias, N.A., 2013. Linear Quadratic Regulator (LQR) controller design for Inverted Pendulum (Doctoral dissertation, Universiti Tun Hussein Malaysia). pp. 1-90.

[4] Savaresi, S.M., Poussot-Vassal, C., Spelta, C., Sename, O. and Dugard, L., 2010. Semi-active suspension control design for vehicles. Elsevier, pp. 1-192.

[5] Önen, Ü., Çakan, A. and İlhan, İ., 2017. Particle swarm optimization based lqr control of an inverted pendulum. Engineering and Technology Journal, 2(5), pp.168-174.

[6] Al-Mahturi, A. and Wahid, H., 2017. Optimal tuning of linear quadratic regulator controller using a particle swarm optimization for a two-rotor aerodynamical system. International Journal of Electronics and Communication Engineering, 11(2), pp.196-202.

[7] Ruderman, M., Krettek, J., Hoffmann, F. and Bertram, T., 2008. Optimal state space control of DC motor. IFAC Proceedings Volumes, 41(2), pp.5796-5801.

[8] Szabolcsi, R., 2018. Design and development of the LQR optimal controller for the unmanned aerial vehicle. Review of the Air Force Academy, (1), pp.45-54.

[9] Burns, R., 2001. Advanced control Engineering. Oxford: Butterworth Heinemann, Jordan Hill, ISBN 0750651008, pp. 272-299.

[10] Hassani, K. and Lee, W.S., 2014, May. Optimal tuning of linear quadratic regulators using quantum particle swarm optimization. In Proceedings of the International Conference on Control, Dynamic Systems, and Robotics (CDSR'14) (Vol. 14, p. 15).

[11] Sen, M.A. and Kalyoncu, M., 2016. Optimal tuning of a LQR controller for an inverted pendulum using the Bees algorithm. J Autom Control Eng, 4(5), pp. 384-387

[12] Hao, Z.F., Guo, G.H. and Huang, H., 2007, August. A particle swarm optimization algorithm with differential evolution. In 2007 international conference on machine learning and cybernetics (Vol. 2, pp. 1031-1035). IEEE.

[13] Zhu, H., Wang, Y., Wang, K. and Chen, Y., 2011. Particle Swarm Optimization (PSO) for the constrained portfolio optimization problem. Expert Systems with Applications, 38(8), pp.10161-10169.

[14] Fourie, P.C. and Groenwold, A.A., 2002. The particle swarm optimization algorithm in size and shape optimization. Structural and Multidisciplinary Optimization, 23, pp.259-267.

[15] Ahmed, H. and Glasgow, J., 2012. Swarm intelligence: concepts, models, and applications. School Of Computing, Queens University Technical Report, pp. 1-38.

[16] Arumugam, M.S. and Rao, M.V.C., 2006. On the performance of the particle swarm optimization algorithm with various inertia weight variants for computing optimal control of a class of hybrid systems. Discrete Dynamics in Nature and Society, 2006(79295), pp. 1-17.

[17] Agharkakli, A., Sabet, G.S. and Barouz, A., 2012. Simulation and analysis of passive and active suspension systems using quarter car model for different road profiles. International Journal of Engineering Trends and Technology, 3(5), pp.636-644.

[18] Ahmed, A.A., 2021. Quarter car model optimization of active suspension system using fuzzy PID and linear quadratic regulator controllers. Global Journal of Engineering and Technology Advances, 6(3), pp.088-097.

[19] Ahmed, M.I., Hazlina, M.Y. and Rashid, M.M., 2016. Mathematical modeling and control of active suspension system for a quarter car railway vehicle. Malaysian Journal of Mathematical Sciences, 10(5), pp.227-241.

[20] Al-Mutar, W.H. and Abdalla, T.Y., 2015. Quarter car active suspension system control using fuzzy controller tuned by PSO. International journal of computer applications, 127(2), pp.38-43.

[21] Jiregna, I. and Sirata, G., 2020. A review of the vehicle suspension system. Journal of Mechanical and Energy Engineering, 4(2), pp. 109-114.

[22] Liu, H., Gao, H. and Li, P., 2013. Handbook of vehicle suspension control systems. Institution of Engineering and Technology, pp. 1-397.

[23] Gupta, A., Nitesh, K. D. & Deepak, A., 2022. Optimization in sliding mode control mechanism for reducing vibrations in the Quarter vehicle using Fuzzy Logic. International Journal of Food and Nutritional Sciences, Vol. 11, No. 1, pp. 3390-3401.

[24] Yang, J., Li, J. and Du, Y., 2006. Adaptive fuzzy control of lateral semi-active suspension for high-speed railway vehicle. In Computational Intelligence: International Conference on Intelligent Computing, ICIC 2006 Kunming, China, August 16-19, 2006 Proceedings, Part II 2 (pp. 1104-1115). Springer Berlin Heidelberg.

[25] Eberhart, R. and Kennedy, J., 1995, October. A new optimizer using particle swarm theory. In MHS'95. Proceedings of the sixth International Symposium on micro machine and human science (pp. 39-43). Ieee.

[26] Reynolds, C.W., 1987, August. Flocks, herds and schools: A distributed behavioral model. In Proceedings of the 14th annual conference on Computer graphics and interactive techniques (pp. 25-34